

Deep Adaptation of Adult-Child Facial Expressions by Fusing Landmark Features

Megan A. Witherow, Manar D. Samad, Norou Diawara,

Haim Y. Bar, and Khan M. Iftekharuddin

Abstract—Imaging of facial affects may be used to measure psychophysiological attributes of children through their adulthood, especially for monitoring lifelong conditions like Autism Spectrum Disorder. Deep convolutional neural networks have shown promising results in classifying facial expressions of adults. However, classifier models trained with adult benchmark data are unsuitable for learning child expressions due to discrepancies in psychophysical development. Similarly, models trained with child data perform poorly in adult expression classification. We propose domain adaptation to concurrently align distributions of adult and child expressions in a shared latent space to ensure robust classification of either domain. Furthermore, age variations in facial images are studied in age-invariant face recognition yet remain unleveraged in adult-child expression classification. We take inspiration from multiple fields and propose deep adaptive FACial Expressions fusing BEtaMix SElected Landmark Features (FACE-BE-SELF) for adult-child facial expression classification. For the first time in the literature, a mixture of Beta distributions is used to decompose and select facial features based on correlations with expression, domain, and identity factors. We evaluate FACE-BE-SELF on two pairs of adult-child data sets. Our proposed FACE-BE-SELF approach outperforms adult-child transfer learning and other baseline domain adaptation methods in aligning latent representations of adult and child expressions.

Index Terms—Facial expression recognition, Feature fusion, Feature selection, Beta distributions, Domain adaptation, Transfer learning, Child expressions

1 INTRODUCTION

FROM infancy to adulthood, facial expressions are a ubiquitous, information-rich component of human social interactions. In Autism Spectrum Disorder (ASD), anomalies in the production and perception of facial expressions inform assessment of psychophysiological traits associated with ASD [1], [2], [3]. ASD is a lifelong diagnosis characterized by impaired communication skills. Individuals with ASD are typically diagnosed within the first few years of life and may undergo intervention and treatment throughout childhood and into adulthood. While early intervention is especially important to improve quality of life for individuals with ASD, continuous assessment and monitoring of symptoms throughout the lifespan is an essential precursor to effective intervention and treatment planning. Models for automated facial expression analysis (FEA) may help support individuals with ASD and clinicians with rapid and objective assessments of ASD-related symptoms.

To better assess communication skills and support lifelong care in ASD, FEA models need to generalize across distinctive expression patterns from early childhood to

adulthood. Developing models robust to age variations is a challenging problem in FEA [4], [5]. Most existing approaches optimize the FEA performance on data sets representing specific age ranges. There has been limited work on classifying facial expressions across age groups. Furthermore, age variations in facial images have been well-studied in facial age estimation and age-invariant face recognition (AIFR), but there has been little cross-pollination among these relevant research areas to improve FEA considering adult-child age variations. In the following sections, we discuss related work on the classification of adult and child expressions and methods from relevant research fields. Then, we propose a novel deep feature adaptation approach to the classification of adult and child expressions inspired by the state-of-the-art domain adaptation learning, facial age estimation, and AIFR literature.

1.1 Related work

1.1.1 Classification of adult & child facial expressions

Existing off-the-shelf FEA tools and research [6], [7], [8], [9], [10] have mostly been developed using adult benchmark data sets [5], [11], [12], [13]. However, facial morphology and kinematics gradually develop throughout childhood [14], [15], resulting in a distribution shift between child and adult expression patterns. For models trained on adult data sets, the distribution shift toward adults poorly generalizes distinctive patterns in child expressions [16], [17], [18], [19]. While benchmark data sets of child facial expressions remain limited, they are growing in number [20], [21], [22], [23]. Therefore, there has been an emerging trend directed at the classification of child facial expressions [16],

• *M.A. Witherow is with the Vision Lab, Department of Electrical & Computer Engineering, Old Dominion University, Norfolk, VA 23529. E-mail: mwith010@odu.edu.*

• *M.D. Samad is with the Department of Computer Science, Tennessee State University, Nashville, TN 37209. E-mail: msamad@tnstate.edu.*

• *N. Diawara is with the Department of Mathematics & Statistics, Old Dominion University, Norfolk, VA 23529. E-mail: ndiawara@odu.edu.*

• *H.Y. Bar is with the Department of Statistics, University of Connecticut, Storrs, CT 06269. E-mail: haim.bar@uconn.edu.*

• *K.M. Iftekharuddin is with the Vision Lab, Department of Electrical & Computer Engineering, Old Dominion University, Norfolk, VA 23529. E-mail: kiftekha@odu.edu.*

[17], [18], [19], which is imperative for the study of children with developmental disorders like ASD. Child facial expressions have been shown to be more exaggerated and varied than those of adults, making child expression classification a more challenging task than adult expression classification [15], [19]. Recently, deep transfer learning using convolutional neural networks (CNNs) has shown promise for the classification of child facial expressions [17], [18], [20]. However, recent studies focus only on maximizing performance on child facial expression benchmarks, bounded by a very limited age range and sample size [5]. Such models tuned for child expressions fail to generalize to adult expressions [19]. To overcome the poor generalization problem across age groups, limited existing work on facial expression classification involving mixed age groups (child, adult, elderly) suggests two primary approaches: (1) curating a mixed age training set to match the age distribution of the test set [24], and (2) classifying images into age groups to determine the age-appropriate classification model for subsequent classification [25]. The first approach requires the age distribution of the test set to be known *a priori* with availability of matching benchmark data. The second approach requires a robust age group classifier to select an appropriate expression classifier model and availability of benchmark data to train expression classifiers for individual age groups. Age group classification is a challenging problem [26], [27] and variations in expression make accurate age estimation even more challenging [25], [28]. Furthermore, it is unclear if age group classification is an adequate preprocessing step as developments in both facial structure and muscle movements contribute to visual differences in child and adult expressions. A child's growth is a gradual process that is uniquely individual, making the transition unclear when a child manifests the full spectrum of adult expressions.

Recently, domain adaptation has shown an interesting pathway to adapt an adult expression classification model using few child expression samples [18]. This approach utilizes a dual stream deep CNN architecture and semantically aligns the class conditional distributions of child and adult domains [18]. The underlying framework of this approach [29] is based on learning a domain-invariant latent representation. Such domain-invariant representations have shown to generalize even to unseen domains [29]. However, while state-of-the-art performance is reported for the target domain, the performance on the source domain is unevaluated [18], [29]. For example, Witherow et al. [18] perform adult to child domain adaptation for child facial expression classification with limited target samples. To maximize target performance, all adult data is used to train. Only child data is held out for evaluation. We hypothesize that learning a domain-invariant representation of expressions may prove effective for facial expression classification across child and adult domains. Consequently, this work proposes a new deep domain adaptation solution to both adult and child expression classification problems that achieves a robust domain-invariant feature representation by selecting landmark features correlated with expressions.

1.1.2 Recognition of age-varying facial images

While limited attention has been given to facial expression classification across age groups, facial age estimation [30] and AIFR [31] are active research areas. Facial age estimation may be framed as either a classification, e.g., age group classification, or regression problem and seeks to associate a categorical or numeric age with a facial image [30]. Meanwhile, the goal of AIFR is to recognize facial identity in the presence of aging variations with applications in locating missing children, biometrics, forensic investigations, and more [31]. State-of-art approaches for facial age estimation and AIFR have benefitted from deep learning and fusion of geometric and texture features [27], [30], [32]. Geometric features derived from facial landmarks capture structural changes associated with childhood development while texture features capture skin artifacts, such as wrinkles, associated with adult aging [27], [32]. Contemporary studies continue to use traditional feature extraction methods, e.g., local binary patterns, histograms of oriented gradients, etc., but recently emphasize deep learning, e.g., CNNs, for texture feature extraction [30], [31], [33]. Common geometric landmark features include distances between landmarks, ratios of distances, and areas and angles of triangles formed by landmark triplets [26], [34], [35], [36], [37]. Similar landmark features, including pairwise distances between landmarks and areas/angles of facial polygons formed by connecting neighboring landmark points, have also been shown to be discriminative for FEA [38], [39], [40], [41]. Therefore, we hypothesize that domain-invariant representation learning of adult and child facial expressions can benefit from a fusion of CNN-extracted and landmark-derived features.

The use of the same feature types in both facial age estimation and AIFR suggests a subset of features correlated with and invariant to age. Statistical latent variable models optimized using the Expectation-Maximization (EM) algorithm have been applied to AIFR to decompose feature sets into age and identity factors [31]. This approach identifies a set of discriminative features for identity recognition using the identity factor, representing facial identity features invariant to age [31]. Gong et al. [42] have first proposed this approach using hidden factor analysis (HFA). HFA assumes the independence of age and identity, which is untrue in practice as different individuals may have different aging patterns [31]. To overcome the independence assumption, the modified HFA (MHFA) approach introduces an additional factor representing age and identity-correlated facial appearance variations [43]. By taking age and identity correlations into account, MHFA has shown to outperform its unmodified counterpart [43]. Given that the appearance of facial expressions varies among individuals and age groups, we hypothesize that FEA can benefit from decomposition of feature sets into those correlated with expression, domain (adult or child), and identity. However, MHFA assumes that data are independent and identically distributed (i.i.d.) following a normal distribution with homogenous variances, which may not be true for real world facial expression data. Furthermore, HFA and MHFA require the optimization of one model per feature, making high dimensional feature vectors computationally

prohibitive [42], [43]. Thus, principal component analysis (PCA) has been used for dimensionality reduction of the feature vector prior to HFA or MHFA [42], [43]. PCA assumes that the features are jointly normally distributed and yields an ordered collection of orthogonal principal components. While PCA guarantees that the first principal components explain more of the variance than subsequent principal components, such linear data projection method does not guarantee that the PCA feature space will be discriminative for classification. Each principal component is a linear combination of all input features, making it less intuitive to understand the contribution of individual features. Moreover, all features, even those with limited contribution to discriminability, are needed to reproduce the same principal components.

Very recently, the Beta-Mixture (BetaMix) method [44] has been proposed to determine significant correlations among large numbers of variables using a mixture of Beta distributions. The method, based on ideas and results from convex geometry, works well even for moderate sample sizes, e.g., $N=10$ depending on the number of predictors, and does not require assumptions of i.i.d., normality, or homogeneity of variances. The BetaMix method detects correlations among all the features at once, so the EM algorithm needs to be applied only once for all features rather than for individual features. Since the BetaMix method is appropriate for large feature vectors, dimensionality reduction is not required and the feature correlations may be interpreted directly, allowing for greater understanding of the interaction between the features and domain, identity, and expression factors. The BetaMix method has shown promising results across multiple applications, including feature selection and classification [44]. We propose the BetaMix method to explore correlations among landmark features and expression, age group, and identity as well as select discriminative features for expression classification.

1.2 Contributions

We propose novel deep domain adaptative FACial Expressions fusing BEtaMix SElected Landmark Features (FACE-BE-SELF) for domain-invariant expression classification. To the best of our knowledge, our proposed deep domain adaptive FACE-BE-SELF approach is the first to perform concurrent adult-child domain adaptation and learn a generalized expression representation that may be used for both child and adult facial expression classification. Our contributions are as follows:

- We fuse facial landmark measurements with deep feature representations for robust expression learning across age groups.
- Our facial landmark features are decomposed based on correlations with expression, domain, and identity factors.
- A novel statistical method based on a mixture of Beta distributions is proposed for facial feature selection for deep learning.
- A new variant of concurrent adult to child expression learning is performed to yield domain-invariant facial expression classification.
- The proposed domain adaptation method is

compared to baseline CNN, transfer learning, and existing domain adaptation methods for facial expression recognition using multiple benchmark data sets.

The remainder of this paper is organized as follows. Section 2 describes the methodology of our approach. Section 3 and 4 present the results and discussion, respectively. Section 5 discusses limitations and Section 6 presents the conclusion.

2 METHODS

2.1 Data sets

We evaluate our proposed method using five data sets of facial expression images: 1) the Extended Cohn-Kanade (CK+) data set [11], [12], 2) the Denver Intensity of Spontaneous Facial Action (DISFA) data set [13], 3) the Extended Denver Intensity of Spontaneous Facial Action (DISFA+) data set [45], 4) the Child Affective Facial Expression (CAFE) data set [21], [22], and 5) the Child Emotion Facial Expression Set (ChildEFES) [23].

2.1.1 CK+ data set

The CK+ data set [11], [12] consists of 593 image sequences of posed facial expressions, including labeled 'anger', 'disgust', 'fear', 'happy', 'sad', 'surprise', and 'contempt' examples, captured from 123 adult subjects (ages 18 to 50 years). A mixture of color and grayscale sequences are present in the data set. Sequences vary in length, but each sequence begins with the neutral expression and ends with the peak expression frame, which has been coded for action units (AUs) from the facial action coding system (FACS). We assign the last three frames of a sequence with its corresponding expression label and label the first frame of each sequence as 'neutral'. This yields 1254 samples: 135 'anger', 177 'disgust', 75 'fear', 207 'happy', 327 'neutral', 84 'sad', and 1369 'surprise'.

2.1.2 DISFA and DISFA+ data sets

The DISFA data set [13] consists of color videos of the spontaneous facial expressions of 27 adult subjects (ages 18 to 50 years) in response to a 4-minute stimulus. The videos are collected at 20 frames per second, and each frame has been coded for FACS AUs. The DISFA+ data set [45] consists of color image sequences of posed facial expressions of nine out of the 27 subjects in the DISFA data set. For each subject, there are 42 different posed facial displays representing a variety of AU combinations. Each sequence frame has been coded for FACS AUs. We sample the DISFA data set at 20 frames per second to generate image sequences. For both DISFA and DISFA+, we assign the expression labels based on the FACS AU codes [11], [46]. We consider the combination of DISFA and DISFA+ as the DISFACat data set. Then, the DISFACat dataset consists of 91281 samples: 637 'anger', 2996 'disgust', 1276 'fear', 11172 'happy', 73376 'neutral', 455 'sad', and 1369 'surprise'.

2.1.3 CAFE data set

The CAFE data set [21], [22] consists of 1192 color photographs of 154 child subjects (ages 2 to 8 years) posing

'anger', 'disgust', 'fear', 'happy', 'sad', and 'surprise' expressions, including 'neutral'. The data set includes open and closed mouth variations for each expression except 'surprise', which is posed with open mouth only. We include the mouth closed variant of all expressions except for 'surprise', yielding 707 samples: 119 'anger', 96 'disgust', 79 'fear', 120 'happy', 129 'neutral', 62 'sad', and 102 'surprise'. The data usage agreement for the CAFE dataset does not allow republication of the images.

2.1.4 ChildEFES data set

The ChildEFES data set [23] consists of color photos and videos capturing 34 child subjects (ages 4 to 6 years) producing a mixture of spontaneous and posed 'anger', 'disgust', 'fear', 'happy', 'sad', 'surprise', and 'contempt' expressions. Expression labels are assigned based on agreement of four FACS judges. We crop the expression-labeled videos to the peak expression. Then, we sample the cropped videos at 20 frames per second to generate image sequences. Since the photographs are a subset of the image sequences, we include only the frames sampled from the videos. This yields 9420 samples: 1435 'anger', 1196 'disgust', 655 'fear', 2196 'happy', 2445 'neutral', 1053 'sad', and 440 'surprise'. The data usage agreement for the ChildEFES data set does not allow republication of the images.

2.1.5 Notation

Let input space \mathcal{X} represent the set of all possible facial images and features. Output space $\mathcal{Y} = \{0, \dots, K - 1\}$ is the set of K expression class labels ('anger', 'disgust', 'fear', 'happy', 'neutral', 'sad', 'surprise'). \mathcal{X} and \mathcal{Y} are related by a function $f: \mathcal{X} \rightarrow \mathcal{Y}$. We consider adult facial expressions (CK+, DISFACat) as the source domain and child facial expressions (CAFE, ChildEFES) as the target domain. We represent each source data set as $D_S = \{(x_i^S, y_i^S) \mid x_i^S \in \mathcal{X}, y_i^S \in \mathcal{Y}\}_{i=1}^{N_S}$, $x_i^S \sim p_X^S$ where N_S is the total number of samples and p^S is the source probability distribution. We represent each target data set as $D_T = \{(x_i^T, y_i^T) \mid x_i^T \in \mathcal{X}, y_i^T \in \mathcal{Y}\}_{i=1}^{N_T}$, $x_i^T \sim p_X^T$ where N_T is the total number of samples and p^T is the target probability distribution.

2.2 Preprocessing

Data sets are preprocessed following [17]. The dlib (<http://dlib.net/>) library is used to detect the face in each image and extract landmark coordinates on the face. The landmarks are used to center and rotate the face so that the eyes are level. The images are cropped such that the left eye is located 30% of the image width in pixels from the left edge. Images are resized to 256 by 256 pixels, converted to grayscale, and normalized to range [0, 1].

2.3 Feature extraction

Using the dlib library, we extract landmark points located at and around facial features such as the nose, eyes, mouth, and eyebrows as well as the perimeter of the face. These landmark locations are used to derive geometric features from FEA and AIFR literature based on pairs and triplets of landmarks. Inter-landmark distance features [27], [34], [36], [37], [41] are measured as the Euclidean distance between pairs of landmarks. Facial triangles [35], [36], [40] are extracted based on a Delaunay triangulation over the

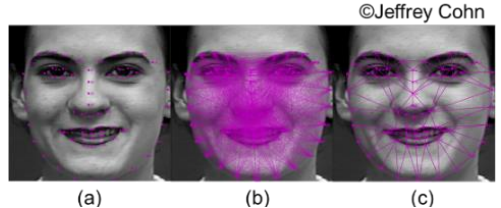


Fig. 1. Sample image overlaid with: (a) facial landmark points, (b) inter-landmark distance features, (c) Delaunay triangulation of the face. ©Jeffrey Cohn

landmark locations. Each triangle is represented by a landmark triplet and has four associated features: the area of the triangle and its three angles expressed in radians. Fig. 1 shows examples of the extracted features.

2.4 Landmark feature decomposition and selection

We fit the BetaMix method [44] to find significant correlations between extracted features from adult-child data and three experimental factors taken from the labeled data: expression, domain, and identity. Extracted features for the source and target data sets are concatenated to form a matrix of P predictors and N samples, where $P > N$. Expression, domain, and identity are represented using three additional predictor variables. We assume the data as P points in \mathbb{R}^N . Subspaces of \mathbb{R}^N lie on the Grassmann manifold, a special type of Riemannian manifold with a nonlinear structure [44]. The Grassmann manifold $\mathbb{G}_{N,d}$ is used to study d -dimensional subspaces of \mathbb{R}^N [44]. Principal angles $(\theta_1, \dots, \theta_d)$ between d and l -dimensional subspaces in $\mathbb{G}_{N,d}$ have an invariant measure for $d \leq l$ that can be used to compute the volume and probability of their sets [44]. These principal angles can be used to determine canonical correlations (ρ_1, \dots, ρ_d) as $\rho_k = \cos \theta_k$ with pairs of canonical variables $\{\varphi_k, \phi_k\}_{k=1}^d$ where $\varphi_k \in \mathbb{G}_{N,d}$, $\phi_k \in \mathbb{G}_{N,l}$ [44]. When $d = l = 1$, $\mathbb{G}_{N,1}$ corresponds to lines through the origin of Euclidean space [44]. The line is a natural choice of projection due to its computational ease and interpretability. Furthermore, when $d = l = 1$, the random variable $\sin^2 \theta$ has the following Beta distribution [44]:

$$\lambda \stackrel{\text{def}}{=} \sin^2 \theta \sim \text{Beta}\left(\frac{N-1}{2}, \frac{1}{2}\right), \quad (1)$$

Thus, we consider that predictors lie on $\mathbb{G}_{N,1}$ and define θ_k as the angle between the k th pair of predictors, $k = 1, \dots, P(P-1)/2$ [44]. We let $\lambda_k = \sin^2 \theta_k$. A predictor is considered 'null' if it corresponds to a randomly sampled point in \mathbb{R}^N . As shown in [44], pairs of null predictors are expected to be mutually perpendicular with high probability, even for moderate values of N . In relation to (1), a mixture of Beta distributions may be used to determine if the pair of predictors represented by each λ_k are 'null' (uncorrelated) or 'nonnull' (correlated). Then, the BetaMix model is defined as:

$$l(\lambda_k) = \iota_{0,k} d_0(\lambda_k) + (1 - \iota_{0,k}) d(\lambda_k), \quad (2)$$

where $d_0(\lambda_k)$ is the null distribution, $d(\lambda_k)$ is the alternative distribution, $\iota_{0,k} \sim \text{Ber}(p_0)$ is a random indicator that equals one if the k th pair of predictors corresponding to λ_k are 'null', and p_0 is the probability of the 'null' component. The 'null' component of the mixture model is defined by the Beta distribution:

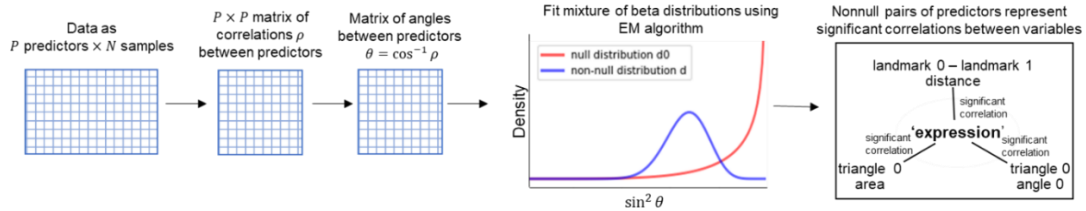


Fig. 2. Overview of the BetaMix method. Data is entered as a matrix of P predictors and N samples. Correlations ρ between the predictors are computed and $\theta = \cos^{-1} \rho$ is used to compute the pairwise angles between predictors from the correlations. Next, the EM algorithm is used to fit a mixture of Beta distributions over random variables $\sin^2 \theta$. Pairs of predictors are considered ‘nonnull’ if the posterior null probability under d_0 is smaller than a threshold. These ‘nonnull’ pairs represent significant correlations between variables. The ‘nonnull’ pairs for expression, domain, and identity are used to decompose the feature vector into sets correlated with each of the three factors.

$$d_0(\lambda_k) = \frac{1}{\text{Beta}(\frac{s-1}{2}, \frac{1}{2})} \lambda_k^{\frac{s-1}{2}-1} (1 - \lambda_k)^{\frac{1}{2}}, \quad (3)$$

where $s \leq N$ is the estimated effective sample size. The ‘nonnull’ component of the mixture model is defined as:

$$d(\lambda_k) = \frac{1}{\text{Beta}(\alpha, \beta)} \lambda_k^{\alpha-1} (1 - \lambda_k)^{\beta-1}, \quad (4)$$

where $\alpha, \beta > 0$. The latent mixture variables (α, β, s) are estimated using the EM algorithm. The E-step updates ι_{0k} with the posterior mean:

$$\hat{\iota}_{0k} = \frac{p_0 d_0(\lambda_k)}{p_0 d_0(\lambda_k) + (1 - p_0) d_0(\lambda_k)} \quad (5)$$

and p_0 is updated with its maximum likelihood estimate, $\hat{p}_0 = \mathbb{E}(\hat{\iota})$. The M-step obtains the maximum likelihood estimates of α, β , and s by solving the following equations:

$$\psi(\alpha) - \psi(\alpha + \beta) = \frac{\sum_{k=1}^{P(P-1)/2} (1 - \iota_{0k}) \log(\lambda_k)}{\sum_{k=1}^{P(P-1)/2} (1 - \iota_{0k})} \quad (6)$$

$$\psi(\beta) - \psi(\alpha + \beta) = \frac{\sum_{k=1}^{P(P-1)/2} (1 - \iota_{0k}) \log(1 - \lambda_k)}{\sum_{k=1}^{P(P-1)/2} (1 - \iota_{0k})} \quad (7)$$

$$\psi\left(\frac{s-1}{2}\right) - \psi\left(\frac{s}{2}\right) = \frac{\sum_{k=1}^{P(P-1)/2} \iota_{0k} \log(\lambda_k)}{\sum_{k=1}^{P(P-1)/2} \iota_{0k}} \quad (8)$$

where $\psi(\cdot)$ is the digamma function. The E- and M-steps are repeated iteratively to update the parameters until convergence. Pairs of predictors are considered ‘nonnull’ if the posterior null probability under d_0 is smaller than threshold τ , $\hat{\iota}_{0k} < \tau$. Fig. 2 summarizes the BetaMix method.

Based on the ‘nonnull’ pairs for each factor, we decompose the feature vector into sets correlated with expression, domain, and identity. For our proposed FACE-BE-SELF approach, we select the features correlated with expression for use in subsequent feature fusion.

2.5 Deep Learning Models

We model supervised classification as the inverse problem:

$$Y = f(X; w) \quad (9)$$

where $f(\cdot)$ is a neural network model parameterized by weights w , $X \in \mathcal{X}$ are the model inputs, and $Y \in \mathcal{Y}$ are the class labels. We partition $f(\cdot)$ into a feature extractor $M: \mathcal{X} \rightarrow Z$ and a classifier $C: Z \rightarrow \mathcal{Y}$ such that $f = C \circ M$ with latent feature space Z . Using this notation, we define multiple architectures: a multi-layer perceptron (MLP), CNN, and feature fusion model with MLP and CNN components.

For the MLP, we consider $X = V$, where feature set $V \in$

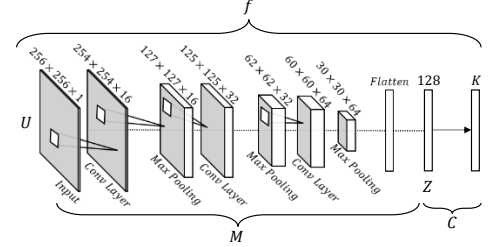


Fig. 3. CNN architecture. Model $f(\cdot)$ is partitioned into feature extractor $M(\cdot)$, mapping from input $U \in \mathbb{R}^{256 \times 256}$ to latent feature vector Z , and classifier $C(\cdot)$, mapping from Z to the K -dimensional output.

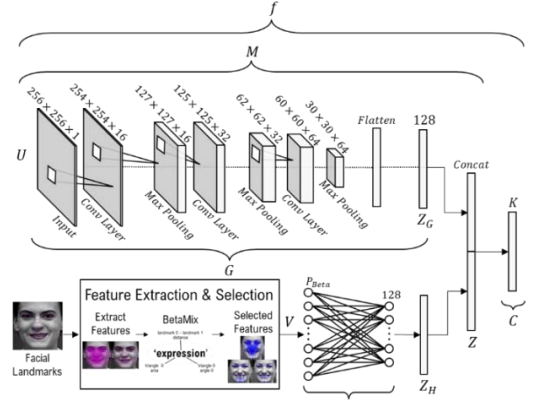


Fig. 4. Feature fusion architecture. Model $f(\cdot)$ is partitioned into feature extractor $M(\cdot)$ and classifier $C(\cdot)$. $M(\cdot)$ consists of CNN model $G: U \rightarrow Z_G$ and MLP $H: V \rightarrow Z_H$. Z_G and Z_H are concatenated as Z and classifier $C(\cdot)$, maps from Z to the K -dimensional output.

$V = \mathbb{R}^{P_{Beta}}$ and P_{Beta} is the number of BetaMix-selected features based on significant correlations with expression. We consider a latent feature vector $Z \in \mathcal{Z} = \mathbb{R}^{128}$ produced at the final hidden layer of the MLP. The output layer has K nodes, representing the number of class labels.

For the CNN, we consider $X = U \in \mathcal{U} = \mathbb{R}^{256 \times 256}$ and define $M(\cdot)$ as a sequence of three convolutional blocks, each consisting of a convolutional layer with 3×3 filter kernels followed by 2×2 maximum response pooling, and a fully connected neural network with a 128-dimensional hidden layer. This hidden layer yields a latent feature vector $Z \in \mathcal{Z} = \mathbb{R}^{128}$. We define $C(\cdot)$ as a fully connected layer mapping $Z \rightarrow \mathcal{Y}$. This CNN architecture is shown in Fig. 3.

For our proposed FACE-BE-SELF feature fusion model, we define X as a tuple (U, V) , where $U \in \mathcal{U} = \mathbb{R}^{256 \times 256}$ and $V \in \mathcal{V} = \mathbb{R}^{P_{Beta}}$. Feature extractor $M(\cdot)$ is made up of CNN model $G: U \rightarrow Z_G$, $Z_G = \mathbb{R}^{128}$ and the MLP model $H: V \rightarrow Z_H$, $Z_H = \mathbb{R}^{128}$. We define the concatenation of Z_G and Z_H spaces as $Z \in \mathcal{Z} = \mathbb{R}^{256}$. Then, we define $C(\cdot)$ as a fully connected layer mapping from Z onto \mathcal{Y} . The architecture of the feature fusion model is shown in Fig. 4.

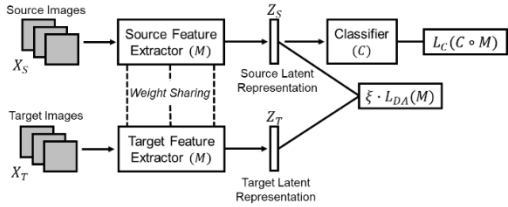


Fig. 5. Domain adaptation framework. Source-target pairs (X_S, X_T) are passed into parallel feature extractors $M(\cdot)$, which share weights. Resulting latent distributions are aligned using domain alignment loss L_{DA} . Classifier $C(\cdot)$ is supervised by classification loss L_C .

2.6 Deep Domain Adaptation

Rather than maximizing the performance on a target domain, our goal for deep domain adaptation is to optimize the model for maximum performance on both source and target domains. We assume the distribution shift between source and target domains can be attributed to covariate shift $p_X^S(x) \neq p_X^T(x)$, rather than a shift in the label distributions, i.e., $\forall x \in \mathcal{X}, p^S(Y|X=x) = p^T(Y|X=x)$. We adopt a dual stream architecture (Fig. 5) consisting of parallel feature extractors $M_S(\cdot)$ and $M_T(\cdot)$ for source and target distributions, respectively. Weights are shared between the two branches such that $M(\cdot) = M_S(\cdot) = M_T(\cdot)$. Paired source and target examples X_S and X_T are passed into respective feature extractors to yield source and target latent representations, i.e. $Z_S = M(X_S)$ and $Z_T = M(X_T)$. Classifier $C(\cdot)$ is trained with Z_S and Z_T in alternating batches to optimize performance on both source and target domains. We use biased batch sampling to ensure that each expression class has equal probability of being represented in each batch.

The model is optimized using two supervised loss functions: classification loss $\mathcal{L}_C(f)$ and domain alignment loss $\mathcal{L}_{DA}(M)$. We define \mathcal{L}_C as the categorical cross-entropy loss due to the multiclass expression classification problem. We define \mathcal{L}_{DA} as the contrastive alignment loss [29]:

$$\begin{aligned} \mathcal{L}_{DA}(M) = & \sum_{a=1}^K \sum_{i,j} d(M(x_i^S|y_i^S=a), M(x_j^T|y_j^T=a)) \\ & + \sum_{a,b|a \neq b}^K \sum_{i,j} k(M(x_i^S|y_i^S=a), M(x_j^T|y_j^T=b)) \end{aligned} \quad (10)$$

We follow [29] in selecting $d(\cdot)$ and $k(\cdot)$ as:

$$d(M(x_i^S), M(x_j^T)) = \frac{1}{2} \|M(x_i^S) - M(x_j^T)\|_F^2 \quad (11)$$

and

$$\begin{aligned} k(M(x_i^S), M(x_j^T)) & \\ & = \frac{1}{2} \left(\max(0, m - \|M(x_i^S) - M(x_j^T)\|_F) \right)^2 \end{aligned} \quad (12)$$

where $\|\cdot\|_F$ is the Frobenius norm and margin $m = 1$ [29]. The effect of \mathcal{L}_{DA} is to minimize 1) distance between samples of the same class from different domains, and 2) similarity between samples of different classes and domains. The overall loss is:

$$\mathcal{L} = \mathcal{L}_C + \xi \mathcal{L}_{DA}, \quad (13)$$

where $0 < \xi < 1$ is a scaling parameter for balancing the contribution of domain alignment loss.

2.7 Experiments

We preprocess the CAFE, ChildEFES, CK+, and DISFACat data sets following Section 2.2. To evaluate our proposed FACE-BE-SELF method, we consider data sets in two

source/target pairs: CK+/CAFE (posed expressions only) and DISFACat/ChildEFES (mixture of posed and spontaneous expressions). We split each data set into multiple train and test sets via bootstrapping. Due to the visual similarities of images in video frames of the same subject, the data split is important to ensure that the same subject does not appear in both train and test sets [17], [18]. For the source CK+ and target CAFE data sets, we randomly split images into 90% train and 10% test sets. Then, we split the 90% train set into 80% train and 10% validation sets. We repeat this process to generate three bootstrapped train/validation/test sets. For the source DISFACat and target ChildEFES data sets, we randomly select subjects for the test set until all classes are represented. Then, we randomly sample 2000 images from the remaining subjects to form the train set.

We fit the BetaMix method on the train sets for each source/target pair. We use the default value of $\tau = 0.01$ as the null posterior probability threshold. Fitting the model yields the mean number and overlap of correlated features for expression, domain, and identity. Expression-correlated features are selected for subsequent fusion. We assess the discriminability of our data-driven FACE-BE-SELF by comparing expression classification performance against 1) all features and 2) features selected using a default correlation coefficient threshold of 0.5.

We investigate the performance of different deep domain adaptation architectures on the validation set and select the best architecture for reporting our results. The validation set is used to select a value for the loss balancing parameter ξ (Equation 13). Other studies [47], [48] have found that ξ is problem-specific and consider values in the range (0.00, 1.00). Due to high computational costs, we choose among representative low (0.01), moderate (0.3), and high (0.8) values in the range (0.00, 1.00). The same validation set is used to investigate the effect of initializing the domain adaptation model with weights of the model trained on source data, which has been reported to improve performance in [18]. Then, we evaluate the performance of our proposed domain adaptation with FACE-BE-SELF approach on two source/target data set pairs and compare against four baseline models: 1) CNN trained on source data (source CNN), 2) CNN trained on target data (target CNN), 3) two transfer learning approaches (with and without layer freezing), and 4) two existing domain adaptation approaches [18], [29]. For all experiments, we train deep models using the ADAM optimizer, choosing a learning rate of $\zeta = 10^{-3}$ and batch size $n = 32$.

3 RESULTS

3.1 Feature extraction

We extract 68 landmark points on the face as shown in Fig 1(a) and use these to measure inter-landmark distances. Because the 68×68 Euclidean distance matrix is symmetric with zeros (self-distance) in diagonal entries, the total number of inter-landmark distance features is $(68 \text{ landmarks} \times 68 \text{ landmarks}) - 68 / 2 = 2278$. Fig. 1(b) overlays all possible inter-landmark distance features on the face. The Delaunay triangulation over the landmark

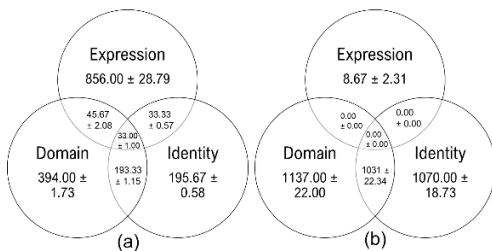


Fig. 6. Mean number of features correlated with expression, domain, and identity for (a) CK+/CAFE and (b) DISFACat/ChildEFES.

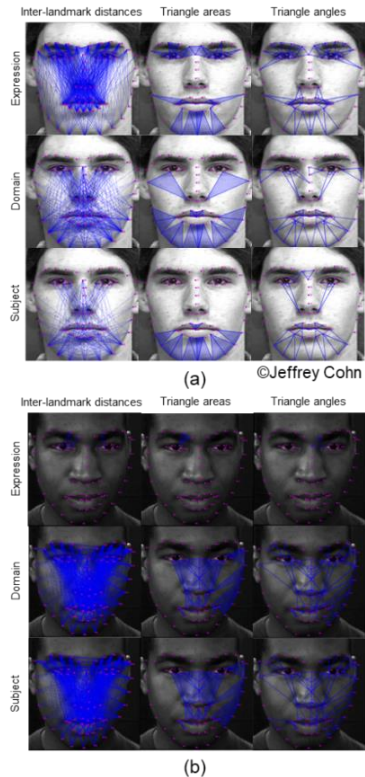


Fig. 7. Features correlated with expression, domain, and identity factors for (a) CK+/CAFE and (b) DISFACat/ChildEFES.

locations results in a set of 106 triangles on the face. For each facial triangle, the area and three internal angles are computed, resulting in $106 \text{ triangles} \times (4 \text{ features/triangle}) = 424$ triangle-based features. Fig. 1(c) visualizes the Delaunay triangulation on the face.

3.2 Selection of landmark features for expression, domain, and identity factors

Fitting the BetaMix method, features are considered significantly correlated with domain, identity, and expression factors if $\sin^2(\theta) > 0.90$. This is equivalent to an angle of 72° or less between the factors and feature, or a correlation coefficient of at least $\rho = \cos(72^\circ) = 0.30$. Fig. 6 shows the mean number of features correlated with 'expression', 'domain', and 'identity', as well as the number correlated with two out of three and all three factors. Fig. 7 illustrates features correlated with the expression, domain, and identity factors for a representative bootstrap set.

Table 1 compares the validation performance of an MLP trained using FACE-BE-SELF with those trained using all features and features selected via an arbitrary thresholding (>0.05) on correlation coefficient with expressions.

TABLE 1
MEAN VALIDATION ACCURACY OF MLP TRAINED WITH DIFFERENT FEATURE SELECTIONS

Dataset	Feature Selection		
	Correlation coefficient > 0.5	BetaMix	All
CAFE	$20.31\% \pm 8.12\%$	$64.58\% \pm 2.39\%$	$17.71\% \pm 2.39\%$
CK+	$41.98\% \pm 22.18\%$	$64.06\% \pm 3.13\%$	$17.71\% \pm 2.39\%$

TABLE 2
MEAN VALIDATION ACCURACY FOR DIFFERENT MODEL ARCHITECTURES

Dataset	MLP	CNN	Feature Fusion
CAFE	$67.71\% \pm 2.39\%$	$80.21\% \pm 3.61\%$	$82.81\% \pm 2.71\%$
CK+	$79.32\% \pm 4.30\%$	$99.38\% \pm 0.41\%$	$99.74\% \pm 0.45\%$

3.3 Domain Adaptation

Table 2 compares the mean validation accuracies of three model architectures: MLP with landmark features, CNN with image features, and CNN with the proposed dual stream architecture for FACE-BE-SELF feature fusion (Fig. 4). CNN performs substantially better than MLP as expected. The FACE-BE-SELF feature fusion model offers additional improvement over the CNN without such fusion. Therefore, we select CNN with our feature fusion setup for subsequent domain adaptation experiments. The mean validation accuracies for three settings of ξ , 0.01, 0.3, and 0.8, are $79.17\% \pm 7.22\%$, $73.96\% \pm 9.02\%$, and $72.92\% \pm 1.80\%$, respectively. We select $\xi = 0.01$ because it produces the best validation accuracy. The mean validation accuracy of the model initialized by sampling from a uniform distribution is $79.17\% \pm 1.80\%$ while initializing with pretrained source weights yields $73.96\% \pm 3.61\%$. We select the initialization with uniform distribution based on the higher mean validation accuracy.

Table 3 and Table 4 compare the mean source and target test accuracies for the CK+/CAFE and DISFACat/ChildEFES source/target pairs, respectively. The comparison models include: 1) source CNN, 2) target CNN, 3) CNN initialized with pretrained source weights and then finetuned on target data (transfer learning without layer freezing), 4) CNN trained via source-to-target transfer learning and finetuned on target data (transfer learning with layer freezing), 5) Motiian et al. [29], and 6) Witherow et al. [18]. Fig. 8 and Fig. 9 compare representative confusion matrices produced by transfer learning with layer freezing and our proposed domain adaptation method for the source/target data set pairs, respectively. Our proposed FACE-BE-SELF method yields higher mean source and target accuracies for both CK+/CAFE (Table 3) and DISFACat/ChildEFES (Table 4) than all baseline methods. Our approach achieves the highest mean accuracy on the CAFE data set, exceeding transfer learning with layer freezing performance by 1.37% on average with lower standard deviation, while maintaining a competitive mean accuracy of 99.71% on CK+, which is 18.24% higher than transfer learning with lower standard deviation (Table 3).

TABLE 3
MEAN TEST ACCURACIES OF COMPARISON MODELS FOR
CK+/CAFE PAIR OF DATASETS

Model	CAFE	CK+
CNN trained on CK+	54.99% \pm 2.43%	99.73% \pm 0.46%
CNN trained on CAFE	91.79% \pm 5.31%	57.59% \pm 10.22%
CNN initialized with CK+ weights, trained on CAFE	91.79% \pm 5.31%	81.47% \pm 3.86%
CNN, CK+ to CAFE transfer learning, fine-tuning on CAFE	91.22% \pm 5.31%	88.47% \pm 6.31%
Motiiian et al. (2017)	89.81% \pm 4.35%	99.17% \pm 0.05%
Witherow et al. (2020)	90.75% \pm 4.64%	99.46% \pm 0.46%
Ours	92.59% \pm 4.63%	99.71% \pm 0.51%

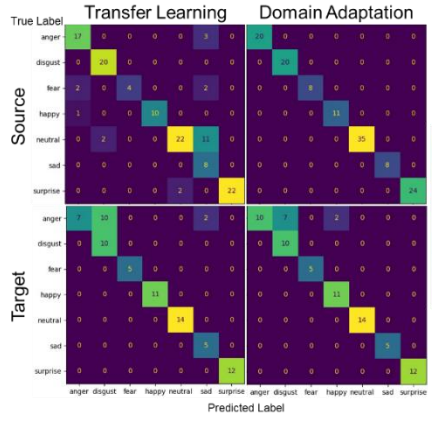


Fig. 8. Representative confusion matrices produced by transfer learning (fine-tuning on target data) and the proposed domain adaptation method for the CK+/CAFE pair of data sets.

4 DISCUSSION

This paper presents a robust classification of adult and child facial expressions through deep domain adaptation and fusion of facial landmark features correlated with expressions. Our experiments on four data sets and comparison of five facial expression classification methods reveal five important findings as follows. First, the decomposition of landmark features for expression, domain, and identity factors reveals common features that are correlated with both expressions and domains (adult versus child) for the CK+/CAFE data set pair, which is not observed with the DISFACat/ChildEFES data set pair (Fig. 6). Features concurrently correlated with expression and domain factors indicate the presence of domain shift in the landmark feature space $\mathcal{V} = \mathbb{R}^{P_{Beta}}$, explaining the need for domain adaptation of the landmark features. While the CNN feature space is known to exhibit adult-child domain shift [16], [17], [18], [19], our results suggest that domain shift is dependent on the domain data set pair. The underlying data dependency of the proposed method may be attributed to differences in sample size, demographics, age ranges, and/or mixture of posed/spontaneous expressions [4], [5]. Second, BetaMix provides a data-driven method to learn a minimum threshold for the correlation coefficient (0.30) between landmark features and the expression factor for selecting the most expression-relevant features instead of using an arbitrary threshold of 0.5 or no feature selection at all (Table 1). Third, the fusion of these BetaMix selected landmark features and CNN-extracted image features improve expression classification

TABLE 4
MEAN TEST ACCURACIES OF COMPARISON MODELS FOR
DISFACAT/CHILDEFES PAIR OF DATASETS

Model	ChildEFES	DISFACat
CNN trained on DISFACat	48.76% \pm 0.62%	98.12% \pm 0.28%
CNN trained on ChildEFES	99.27% \pm 0.19%	43.44% \pm 3.87%
CNN initialized with DISFACat weights, trained on ChildEFES	99.34% \pm 0.10%	74.21% \pm 5.46%
CNN, DISFACat to ChildEFES transfer learning, fine-tuning on ChildEFES	99.41% \pm 0.11%	81.10% \pm 4.31%
Motiiian et al. (2017)	98.24% \pm 0.23%	96.90% \pm 0.36%
Witherow et al. (2020)	98.23% \pm 0.16%	96.85% \pm 0.47%
Ours	98.41% \pm 0.20%	97.41% \pm 0.39%

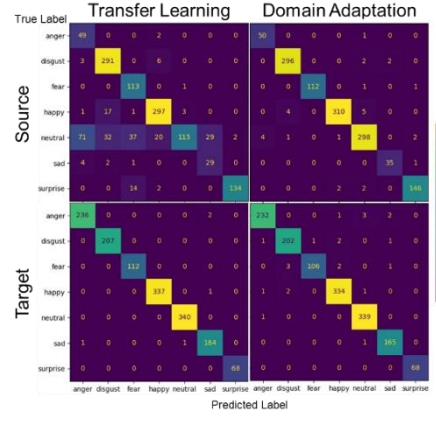


Fig. 9. Representative confusion matrices produced by transfer learning (fine-tuning on target data) and the proposed domain adaptation method for the DISFACat/ChildEFES pair of data sets.

performance for both child and adult data individually compared to baseline CNN and MLP models (Table 2). Fourth, all domain adaptation methods (ours, Witherow et al. [18], Motiiian et al. [29]) substantially outperform adult-to-child transfer learning in adult expression classification (Tables 3, 4). However, the child expression results of domain adaptation are on par with the transfer learning method (Tables 3, 4). This suggests that domain adaptation methods provide a more generalizable or domain (adult versus child) invariant representation of expressions than transfer learning. Fifth, our proposed FACE-BE-SELF method outperforms all baseline domain adaptation methods without feature fusion (Witherow et al. [18], Motiiian et al. [29]), adult-to-child transfer learning with or without frozen layers, and CNN trained on adult or child expression images only (Tables 3, 4). The superiority of our FACE-BE-SELF model is observed in classifying adult only and child only expressions. The following sections provide detailed discussions in addition to and expanding upon these five key findings.

4.1 Data set specific trends in feature and factor correlation

Visualization of landmark features significantly correlated with domain, identity, and expression factors helps explain the relationship between expression-correlated features and domain (Fig. 7). Features concurrently correlated with both expression and domain factors are in the lower portion of the face, at or below the mouth. These features encode information about the movement of the lips, critical for distinguishing between different expressions. In the context of domain, these features represent developmental

changes in lower face proportions from childhood to adulthood [14], [15]. This developmental change may contribute to the domain-shift in landmark feature space $\mathcal{V} = \mathbb{R}^{P_{Beta}}$ to distinctively characterize facial expressions of adults and children.

Features correlated with only the expression factor are consistent across domain and identity. These include features located around the eyes and eyebrows (Fig. 7). This observation is present for both CK+/CAFE and DISFACat/ChildEFES source/target pairs. Such correlations highlight the importance of the eyes and eyebrows in several domain-invariant expressions: furrowing of the brows and tightening of the lids in ‘anger’; wrinkling the nose changing the appearance of the inner corners of the eyes in ‘disgust’; furrowing the brows while raising inner brow, upper brow, and upper eyelid in ‘fear’; tightening of the outer corners of the eyes in ‘happy’; furrowing the brows while raising the inner brow in ‘sad’; and raising the inner brow, outer brow, and upper eyelid in ‘surprise’. In the CK+/CAFE pair, the expression-correlated features are between deformable regions of the face, e.g., eyes, eyebrows, lips, and static facial regions, e.g., nose, outer perimeter of the face (Fig. 7). These correlations are meaningful because expressions are the result of muscle-activated deformations in the facial surface. Unlike expression-correlated features, features correlated with domain and identity factors tend to be between static facial regions, e.g., facial widths, distance between eyes, and angles between eyes and corners of the nose (Fig. 7). These findings are present in both data set pairs and reflect known patterns of craniofacial growth from childhood to adulthood (Fig. 7): increasing height of the inner face, increasing width of the lower face, and changes in nose and mouth proportions [14].

4.2 Selection and fusion of facial landmark features

Our comparison of three feature selection schemes: data-driven with BetaMix, arbitrary thresholding, and no feature selection reveals that our data driven approach yields the most effective selection of features (Table 1). Furthermore, fusing CNN-extracted features with FACE-BE-SELF improves the classification performance of child and adult facial expressions (Table 2). Like age estimation and AIFR, facial expression classification benefits from the fusion of geometric landmark and texture features [30], [31]. Given that the feature fusion model outperforms CNN features only, our selected expression-correlated landmark features provide complementary information representative of expressions beyond that learned by CNN (Table 2). The data-driven minimum correlation coefficient threshold learned by BetaMix preserves useful complementary information for expressions that may be discarded using an arbitrary larger threshold (Table 1). Unlike CNN features, our landmark features are explainable (Fig. 7), allowing features to be traced back to specific facial regions, as discussed in 4.1. Therefore, both the explainability and effectiveness of selected features in classification suggest that the proposed BetaMix correlation coefficient threshold is an effective metric in optimizing feature selection for facial expression classification. Fusing deep features with explainable facial landmark features enables us to achieve superior

classification performance and better explainability of our model.

4.3 Domain adaptation versus transfer learning for expression learning

Our findings suggest that domain adaptation methods considered in this study (ours, Witherow et al. [18], Motian et al. [29]), provide more robust representation learning of adult and child facial expressions compared to adult-to-child transfer learning fine-tuned on child expressions (Tables 3, 4). During adaptation, source and target performance are jointly optimized via \mathcal{L}_C by training on pairs of child and adult images while the class conditional distributions are aligned via \mathcal{L}_{DA} . This optimization procedure ensures robust performance on both domains. Domain adaptation works to yield domain-invariant feature representations by minimizing their correlation with the domain. This is an advantage of FACE-BE-SELF over the MHFA method [43] used in AIFR which only uses age-invariant identity factors for identity recognition, discarding features concurrently correlated with both age and identity. Unlike MHFA, the domain-invariant learning with FACE-BE-SELF allows us to maximize feature correlation with facial expressions while minimizing their correlation with the domain. In this way, we can learn a domain-invariant representation for expressions while still leveraging all expression-relevant information. By contrast, when the source domain representation is tuned to optimize target domain performance during transfer learning, source domain performance deteriorates. Such deterioration may be attributed to the lack of supervision on the adult expression classification task during fine-tuning. Furthermore, transfer learning with layer freezing better preserves representations that are effective for adult expression classification than transfer learning without layer freezing (Tables 3, 4) [17]. The more adult expression-trained weights are fine-tuned on child expressions, the worse the adult expression classification performance is due to domain shift. This suggests that freezing of early layer weights in transfer learning has a protective effect on source domain performance by preventing the learned target classifier from drifting too far from the optimal source classifier. Our findings indicate that joint supervision of source and target classification in domain adaptation while aligning class conditional distributions yields better representations for adult-child expression learning than the sequential pre-training with adult expressions and fine-tuning with child expressions found in transfer learning. The findings also confirm that supervision on both domains or a method of domain alignment is required for effective classification. For both CK+/CAFE and DISFACat/ChildEFES, we observe poor cross domain performance for the CNNs trained on a single domain (Tables 3, 4). This poor cross domain performance is indicative of distribution shift and replicates the findings of multiple prior studies [17], [18], [19].

4.4 Visualizing facial expression shifts

We perform additional analysis to visualize the effect of joint supervision and alignment (domain adaptation with

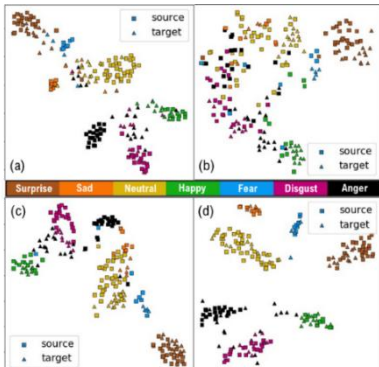


Fig. 10. Representative CK+/CAFE test set plotted using 2D t-SNE embedding of the latent space for multiple comparison models: (a) CNN trained on source data, (b) CNN trained on target data, (c) transfer learning (fine-tuning on target data), and (d) proposed domain adaptation method.

FACE-BE-SELF), supervision on source followed by supervision on target (transfer learning with layer freezing), and single domain learning (adult or child) on the feature space. Fig. 10 and Fig. 11 visualize the class alignment of source and target test samples in the latent space using a t-SNE embedding [49] for CK+/CAFE and DISFACat/ChildEFES, respectively. Fig. 10(a) and Fig. 11(a) show the source samples in distinct clusters by class. While some target samples are aligned by class, e.g., ‘happy’, others are poorly aligned and plotted in the middle of the class clusters. Similarly, Fig. 10(b) and Fig. 11(b) show target samples clustered by class and source samples misaligned. Fig. 10(c) and Fig. 11(c) show that transfer learning produces better class alignment between the source and target samples than CNNs trained on adult or child images only. However, the class clusters are not as tightly coupled or well separated as in Fig. 10(d) and Fig. 11(d) showing that domain adaptation with FACE-BE-SELF yields more effective alignment. Fig. 10(d) and Fig. 11(d) show that FACE-BE-SELF provides a well-aligned domain-invariant representation of child and adult facial expressions.

4.5 Explaining the confusing expression pairs

Fig. 8 reveals that domain adaptation with FACE-BE-SELF and transfer learning with layer freezing both confuse ‘anger’ as ‘disgust’ in the CAFE data set, with transfer learning confusing more than domain adaptation. This may arise from some child subjects wrinkling their noses while posing ‘anger’ since wrinkling of the nose is a visual indicator of the ‘disgust’ expression. Transfer learning also confuses ‘neutral’ as ‘sad’ in the CK+ test set while our domain adaptation approach does not (Fig. 8). Many adults display prominent nasolabial folds (smile lines) even during ‘neutral’ expressions. These nasolabial folds are not seen in ‘neutral’ expressions of children but are visible in child ‘sad’ expressions. Thus, this confusion of ‘neutral’ expression as ‘sad’ expression in the CK+ test set likely arises as a byproduct of fine-tuning on CAFE data. On DISFACat/ChildEFES, the proposed domain adaptation and feature fusion approach matches transfer learning for the highest mean accuracy on ChildEFES with similar standard deviation while achieving 16.31% higher mean accuracy on DISFACat with smaller standard deviation (Table 4). Considering the ChildEFES test set, there are no

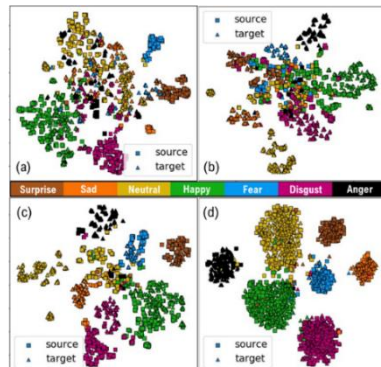


Fig. 11. Representative DISFACat/ChildEFES test set plotted using 2D t-SNE embedding of the latent space for multiple comparison models: (a) CNN trained on source data, (b) CNN trained on target data, (c) transfer learning (fine-tuning on target data), and (d) proposed domain adaptation method.

confused expression pairs in common for either model (Fig. 9). For the DISFACat test set, transfer learning confuses ‘neutral’ samples as other expressions while domain adaptation does not (Fig. 9). We believe that this confusion may be because most images in ChildEFES are spontaneous expressions rather than posed expressions. These child-produced spontaneous expressions are much more subtle than adult expressions in DISFACat. The ‘surprise’ expression suffers from confusion with the neutral expression to a lesser extent because of its unique open-mouth appearance across all four data sets. This explains why the ‘surprise’ expression is one of the least confused expressions for both domain adaptation and transfer learning across all four data sets (Fig. 8, Fig. 9).

5 LIMITATIONS

Although the BetaMix method is robust to dependence among samples, the high degree of similarity among faces (compared to other types of data) and universality of expressions may yield a small effective sample size. Even with a small effective sample size, BetaMix is shown to capture significantly correlated landmark features. However, there may be features that are useful for expression classification but are not significantly correlated with expression based on the BetaMix-learned minimum correlation coefficient. Furthermore, the data dependency of BetaMix feature selections may affect performance on unseen data sets. An additional adaptation or fine-tuning step may be required for these models to address possible data dependency. Age ranges studied cover 2 to 8 years for CAFE, 4 to 6 years for ChildEFES, and 18+ years for CK+ and DISFACat. Further research is required to determine if adapted models are capable of generalizing to participants in other age groups, e.g., teens and pre-teens.

6 CONCLUSION

In this work, we propose for the first time in literature novel deep domain adaptative FACE-BE-SELF for concurrent learning of adult and child facial expressions. FACE-BE-SELF yields a meaningful and effective selection of features that are correlated with expressions. The explainability and visualization of facial landmarks and latent feature

space corroborate the facial expression classification performance of our and other baseline methods. The superiority of our method over existing transfer learning and domain adaption methods concludes the need of a systematic feature selection, feature fusion, and domain adaptation to perform domain-invariant classification. In future work, we plan to investigate the generalizability of this approach to other age groups and data acquisition pipelines. We hope that this approach may be used to yield automated, objective assessments of age or domain varying patterns in other applications.

ACKNOWLEDGMENT

This material is based upon work supported by the National Science Foundation Graduate Research Fellowship under Grant No. 1753793 and by the Research Computing clusters at Old Dominion University under National Science Foundation Grant No. 1828593.

REFERENCES

- [1] K. Owada et al., "Computer-analyzed facial expression as a surrogate marker for autism spectrum social core symptoms," *PLOS ONE*, vol. 13, no. 1, p. e0190442, 2018.
- [2] M. Samad, N. Diawara, J. Bobzien, J. Harrington, M. A. Witherow, and K. Iftekharuddin, "A Feasibility Study of Autism Behavioral Markers in Spontaneous Facial, Visual, and Hand Movement Response Data," *IEEE Transactions on Neural Systems and Rehabilitation Engineering*, vol. 26, no. 2, 2018.
- [3] M. Samad, N. Diawara, J. Bobzien, C. Taylor, J. Harrington, and K. Iftekharuddin, "A pilot study to identify autism related traits in spontaneous facial actions using computer vision," *Research in Autism Spectrum Disorders*, vol. 65, pp. 14-24, 2019.
- [4] S. Bhattacharya and M. Gupta, "A survey on: Facial emotion recognition invariant to pose, illumination and age," presented at the 2019 Second International Conference on Advanced Computational and Communication Paradigms (ICACCP), 2019.
- [5] C. Dalvi, M. Rathod, S. Patil, S. Gite, and K. Kotecha, "A Survey of AI-Based Facial Emotion Recognition: Features, ML & DL Techniques, Age-Wise Datasets and Future Directions," *IEEE Access*, vol. 9, pp. 165806-165840, 2021.
- [6] T. Baltrušaitis, P. Robinson, and L.-P. Morency, "Openface: an open source facial behavior analysis toolkit," presented at the 2016 IEEE Winter Conference on Applications of Computer Vision (WACV), 2016.
- [7] T. Baltrušaitis, A. Zadeh, Y. C. Lim, and L.-P. Morency, "Openface 2.0: Facial behavior analysis toolkit," presented at the 2018 13th IEEE international conference on automatic face & gesture recognition (FG 2018), 2018.
- [8] G. Littlewort et al., "The computer expression recognition toolbox (CERT)," presented at the 2011 IEEE International Conference on Automatic Face & Gesture Recognition (FG), 2011.
- [9] Noldus Information Technology bv. "FaceReader." Noldus Information Technology bv. <https://www.noldus.com/facereader> (accessed 07/27/2022, 2022).
- [10] iMotions A/S. "Facial Expression Analysis." iMotions A/S. <https://imotions.com/biosensor/fea-facial-expression-analysis/> (accessed 07/27/2022, 2022).
- [11] T. Kanade, J. F. Cohn, and Y. Tian, "Comprehensive database for facial expression analysis," presented at the Proceedings Fourth IEEE International Conference on Automatic Face and Gesture Recognition (Cat. No. PR00580), 2000.
- [12] P. Lucey, J. F. Cohn, T. Kanade, J. Saragih, Z. Ambadar, and I. Matthews, "The Extended Cohn-Kanade Dataset (CK+): A complete dataset for action unit and emotion-specified expression," presented at the 2010 IEEE Computer Society Conference on Computer Vision and Pattern Recognition - Workshops, 2010.
- [13] S. M. Mavadati, M. H. Mahoor, K. Bartlett, P. Trinh, and J. F. Cohn, "DISFA: A Spontaneous Facial Action Intensity Database," *IEEE Transactions on Affective Computing*, vol. 4, no. 2, 2013.
- [14] P. Burke and C. Hughes-Lawson, "The growth and development of the soft tissues of the human face," *Journal of anatomy*, vol. 158, p. 115, 1988.
- [15] C. Grossard et al., "Children facial expression production: influence of age, gender, emotion subtype, elicitation condition and culture," *Frontiers in psychology*, p. 446, 2018.
- [16] A. Dapogny et al., "On Automatically Assessing Children's Facial Expressions Quality: A Study, Database, and Protocol," *Frontiers in Computer Science, Original Research* vol. 1, 2019.
- [17] M. Witherow, M. Samad, and K. Iftekharuddin, "Transfer learning approach to multiclass classification of child facial expressions," presented at the SPIE Optical Engineering + Applications, 2019.
- [18] M. Witherow, W. Shields, M. Samad, and K. Iftekharuddin, "Learning latent expression labels of child facial expression images through data-limited domain adaptation and transfer learning," presented at the SPIE Optical Engineering + Applications, 2020.
- [19] Z. Zheng, X. Li, J. Barnes, C.-H. Park, and M. Jeon, "Facial Expression Recognition for Children: Can Existing Methods Tuned for Adults Be Adopted for Children?," presented at the International Conference on Human-Computer Interaction, 2019.
- [20] R. A. Khan, A. Crenn, A. Meyer, and S. Bouakaz, "A novel database of children's spontaneous facial expressions (LIRIS-CSE)," *Image and Vision Computing*, vol. 83-84, 2019.
- [21] V. LoBue and C. Thrasher. The Child Affective Facial Expression (CAFE) set. Databrary. 2014.
- [22] V. LoBue and C. Thrasher, "The Child Affective Facial Expression (CAFE) set: validity and reliability from untrained adults," *Frontiers in Psychology, Methods* vol. 5, 2015.
- [23] J. G. Negrão et al., "The Child Emotion Facial Expression Set: A Database for Emotion Recognition in Children," *Frontiers in Psychology, Original Research* vol. 12, 2021.
- [24] T. G. Rebanowako, A. R. Yadav, and R. Joshi, "Age-Invariant Facial Expression Classification Method Using Deep Learning," presented at the Proceedings of 6th International Conference on Recent Trends in Computing, Singapore, 2021.
- [25] G. Guo, R. Guo, and X. Li, "Facial Expression Recognition Influenced by Human Aging," *IEEE Transactions on Affective Computing*, vol. 4, no. 3, pp. 291-298, 2013.
- [26] R. Angulu, J. R. Tapamo, and A. O. Adewumi, "Age estimation via face images: a survey," *EURASIP Journal on Image and Video Processing*, vol. 2018, no. 1, p. 42, 2018.
- [27] R. Angulu, J. R. Tapamo, and A. O. Adewumi, "Age-Group Estimation Using Feature and Decision Level Fusion," *The Computer Journal*, vol. 62, no. 3, pp. 346-358, 2018.
- [28] Z. Lou, F. Alnajar, J. M. Alvarez, N. Hu, and T. Gevers, "Expression-Invariant Age Estimation Using Structured Learning," *IEEE Transactions on Pattern Analysis and Machine Intelligence*, vol. 40, no. 2, 2018.

[29] S. Motian, M. Piccirilli, D. A. Adjeroh, and G. Doretto, "Unified deep supervised domain adaptation and generalization," presented at the Proceedings of the IEEE international conference on computer vision, 2017.

[30] P. Punyani, R. Gupta, and A. Kumar, "Neural networks for facial age estimation: a survey on recent advances," *Artificial Intelligence Review*, vol. 53, no. 5, 2020.

[31] M. M. Sawant and K. M. Bhurchandi, "Age invariant face recognition: a survey on facial aging databases, techniques and effect of aging," *Artificial Intelligence Review*, vol. 52, no. 2, 2019.

[32] A. S. Osman Ali, V. Sagayan, A. M. Saeed, H. Ameen, and A. Aziz, "Age-invariant face recognition system using combined shape and texture features," *IET Biometrics*, vol. 4, no. 2, 2015.

[33] K. Baruni, N. Mokoena, M. Veeraragoo, and R. Holder, "Age Invariant Face Recognition Methods: A Review," presented at the 2021 International Conference on Computational Science and Computational Intelligence (CSCI), 2021.

[34] M. Sajid, I. A. Taj, U. I. Bajwa, and N. I. Ratyal, "Facial Asymmetry-Based Age Group Estimation: Role in Recognizing Age-Separated Face Images," *Journal of Forensic Sciences*, vol. 63, no. 6, pp. 1727-1749, 2018.

[35] A. Juhong and C. Pintavirooj, "Face recognition based on facial landmark detection," presented at the 2017 10th Biomedical Engineering International Conference (BMEiCON), 2017.

[36] A. Chinnaswamy, P. Kumar, and S. Aravind, "Age Group Estimation using Facial Features," *International Journal of Emerging Technologies in Computational and Applied Sciences*, 2014.

[37] A. Srivastava, "Estimation of Age Groups based on Facial Features," *International Journal of Engineering and Technical Research*, vol. 7, pp. 115-121, 2018.

[38] S. A. Rizwan, A. Jalal, and K. Kim, "An Accurate Facial Expression Detector using Multi-Landmarks Selection and Local Transform Features," presented at the 3rd International Conference on Advancements in Computational Sciences (ICACS), 2020.

[39] M. Murtaza, M. Sharif, M. AbdullahYasmin, and T. Ahmad, "Facial expression detection using Six Facial Expressions Hexagon (SFEH) model," presented at the IEEE 9th Annual Computing and Communication Workshop and Conference (CCWC), 2019.

[40] A. Barman and P. Dutta, "Influence of shape and texture features on facial expression recognition," *IET Image Processing*, vol. 13, no. 8, pp. 1349-1363, 2019.

[41] K. X. Beh and K. M. Goh, "Micro-Expression Spotting Using Facial Landmarks," presented at the IEEE 15th International Colloquium on Signal Processing & Its Applications (CSPA), 2019.

[42] D. Gong, Z. Li, D. Lin, J. Liu, and X. Tang, "Hidden Factor Analysis for Age Invariant Face Recognition," presented at the IEEE International Conference on Computer Vision, 2013.

[43] H. Li, H. Zou, and H. Hu, "Modified Hidden Factor Analysis for Cross-Age Face Recognition," *IEEE Signal Processing Letters*, vol. 24, no. 4, pp. 465-469, 2017.

[44] H. Bar and M. T. Wells, "On Graphical Models and Convex Geometry," *arXiv preprint arXiv:2106.14255*, 2021.

[45] M. Mavadati, P. Sanger, and M. H. Mahoor, "Extended DISFA Dataset: Investigating Posed and Spontaneous Facial Expressions," presented at the 2016 IEEE Conference on Computer Vision and Pattern Recognition Workshops (CVPRW), 2016.

[46] P. Ekman, *Facial action coding system*, Salt Lake City, UT: A Human Face, 2002.

[47] J. N. Kundu et al., "Balancing discriminability and transferability for source-free domain adaptation," in *International Conference on Machine Learning*, 2022: PMLR, pp. 11710-11728.

[48] S. Pei, J. Sun, S. Xiang, and G. Meng, "Domain Decorrelation with Potential Energy Ranking," *arXiv preprint arXiv:2207.12194*, 2022.

[49] L. Van der Maaten and G. Hinton, "Visualizing data using t-SNE," *Journal of machine learning research*, vol. 9, no. 11, 2008.

Megan A. Witherow received her B.S. degree in computer engineering from Old Dominion University (ODU), Norfolk, VA, USA in 2018. She is currently a PhD student at the Vision Laboratory, Dept. of Electrical and Computer Engineering, ODU, and a 2020 NSF Graduate Research Fellow. Her research interests include computer vision, deep learning, human-computer interaction, and affective computing.

Manar D. Samad received the M.S. degree in computer engineering from the University of Calgary, Calgary, AB, Canada in 2011, and the Ph.D. degree from Old Dominion University, Norfolk, VA, USA in 2016. He worked as a post-doctoral fellow at Geisinger Medical Center in Danville, PA for two years. He is currently an Assistant Professor in the Department of Computer Science at Tennessee State University, Nashville, TN, USA. His research interests include machine learning, health informatics, computer vision, and natural language processing.

Norou Diawara is Professor of Statistics in the Mathematics and Statistics Department at Old Dominion University, Norfolk, VA, USA. Prof. Diawara received his B.S. at the University Cheick Anta Diop in Dakar, Senegal; Maîtrise in Mathematics at University of Le Havre, France; Master's in Statistics at University South Alabama; and Ph.D. in Statistics at Auburn University, AL in 2006. His research areas are in estimation techniques of time to event data analyses and neighborhood level causal effects. Such research interests may be included in choice models, statistical pattern recognition using copulas and spatial-temporal models.

Haim Y. Bar received his Ph.D. in statistics at Cornell University in 2012. He received his M.Sc. in statistics in 2010 (Cornell University) and an M.Sc. in computer science in 2002 (Yale University). He received his bachelor degree in mathematics (Cum Laude) in 1993, at the Hebrew University in Jerusalem. His professional interests include statistical modeling, shrinkage estimation, high throughput applications in biology (e.g., genomics), Bayesian statistics, variable selection, and machine learning. From 1995 to 1997, he was with Motorola, Israel, as a computer programmer in the Wireless Access Systems Division. From 1997 until 2003 he worked for MicroPatent, LLC, where he held the position of Director of Software Development. In 2003 he moved to Ithaca, NY, and worked as a Principal Scientist at ATC-NY.

Khan M. Iftekharuddin received the B.Sc. degree in electrical and electronic engineering from the Bangladesh Institute of Technology, Dhaka, Bangladesh, in 1989, and the M.S. and Ph.D. degrees in electrical and computer engineering from the University of Dayton, Dayton, OH, USA, in 1991 and 1995 respectively. He is currently the Associate Dean for Research and Innovation with the Batten College of Engineering and Technology, Old Dominion University (ODU), Norfolk, VA, USA, and the Director of the ODU Vision Laboratory. His current research interests include computational modeling of intelligent systems and reinforcement learning, stochastic medical image analysis, intersection of bioinformatics and medical image analysis, distortion-invariant automatic target recognition, biologically inspired human and machine centric recognition, and machine learning for robotics.